

On the fracture behavior of thin-walled SFRC roof elements

M. di Prisco & D. Dozio

Politecnico di Milano, Milano, Italy

B. Belletti

University of Parma, Parma, Italy

ABSTRACT: Several experimental investigations aimed at the analysis of the structural behaviour of thin walled steel fibre reinforced elements highlighted the effectiveness of design rules suggested in standards, recently proposed for the prediction of serviceability and ultimate limit states, but also a significant interaction between the longitudinal and the crosswise bending of such elements at failure. The interaction due to second order effects is caused by both the open cross-section shape of the prefabricated elements and the reduced thickness of the profiles. The tests correspond to a large scale tests of a strip plate 1m wide and 30m long subjected to an eccentric tension. The shape loss of the cross section drastically anticipated the longitudinal bending collapse. A model based on the equilibrium of a segment assumed perfectly stiff in the cross section plane and a Finite Element approach are compared to explain the onset of the collapse. Very precious indications are pointed out in order to realize what happens in this large scale fracture mechanical test.

1 INTRODUCTION

Fibre reinforced concrete is a promising material when introduced in thin walled structures: a recent research programme carried out by an Italian factory, was aimed at the substitution in prefabricated roof elements of steel welded mesh fabric, made of high bond wires usually adopted as transverse reinforcement, with steel fibres (di Prisco & Felicetti, 1999; di Prisco et al. 2003). The main advantages are related to the thickness reduction connected to the overcoming of cover limitations, the increase of freedom in specimen shape and geometry, that are no longer constrained by reinforcement detailing, and the major industrialization degree reachable in the production process, due to the exclusion of transverse reinforcement handling and placing. The diffused reinforcement is much more well spread and continuously adjustable with respect to steel mesh, limiting the positioning tolerances which can significantly reduce the crosswise bearing of thin webs. The introduction of this material suggests the designer to make the section profile thinner and thinner, thus emphasizing all the problems typical of the high performance materials like instability (di Prisco & Dozio, 2005). The aim of this research is to show how the loads acting on open cross section thin walled elements reproducing snow distribution on

their extrados induce an eccentric tension on the horizontal bottom plate. The huge size of the plate (30m x 1m) subjected to a constant axial force and a variable crosswise bending moment due to vertical load distribution and second order effects can be instrumental in the suggestion of a proper proportioning valid for large thin walled plates made of fibre reinforced concrete. The main point is related to the right design ratio between the ultimate and the cracking resistant bending moment in the crosswise direction.

2 STRUCTURAL TESTS

Three simply supported prefabricated roof elements 30 m long, 2.5 m wide and 1 m deep made of high performance concrete were loaded by means of steel bundles. The reference element, made of conventional R/C, was compared with two Steel Fibre Reinforced Concrete (SFRC) elements. Both the SFRC elements were reinforced with 50 kg/m³ of steel fibres: low and high carbon steel fibres were respectively introduced in the same concrete mix. The total weight of each element was about 24 t; it was characterized by only one closed end. The prestressed reinforcement consisted of 20x0.5" strands.

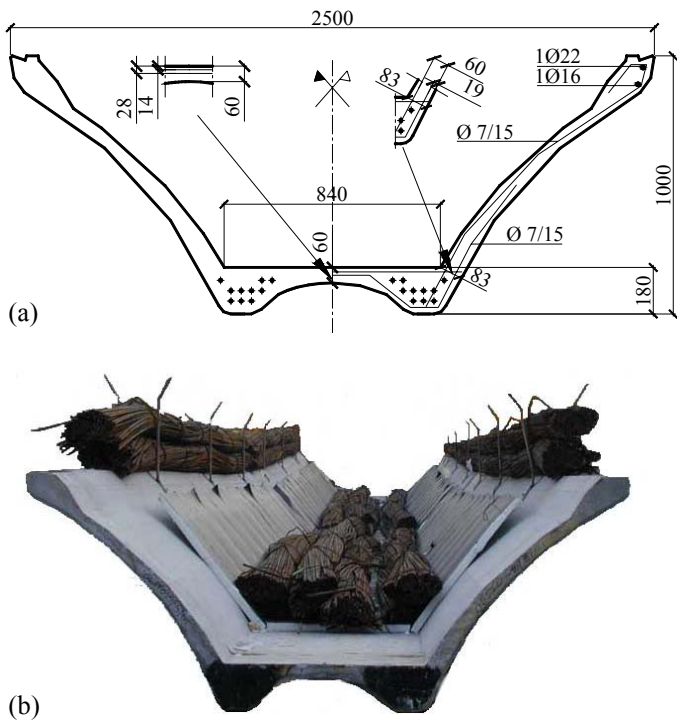


Figure 1. (a) Geometry and structural reinforcement of prefabricated roof elements, (b) loaded cross section.

The prestressed strands were introduced only in the bottom chords (Fig.1a), where a significant fire protection due to thick covers can be achieved.

Two square welded meshes ($2 \times 1 \times \phi 7/150$ mm) located in the wings and in the horizontal slab, guaranteed a geometrical reinforcement ratio of about 8.5‰, in the crosswise direction, in the middle of the slab and 6.2‰ at the bottom of the wings. Each element was widely instrumented in the central section: in fact, the midspan zone was free of any steel bundle for about 1 m. In this section five vertical transducers were located to measure the vertical displacements of the bottom and top chords (Vert_C1, C2, C4, C5; Fig.2a) and one in the middle, at the intrados of the horizontal slab (Vert_C3). Nine resistive transducers measured the longitudinal strains on a gauge length of 500 mm ($EL_C1 \div C9$; Fig.2b) and six resistive transducers measured the transversal strains in two sections t 350 mm from the middle section, at the intrados, on a gauge length of 200 mm ($ET_CD1 \div CD6$; Fig.2b), while further three resistive transducers measured the transverse strain in the middle section at the extrados, always on a gauge length of 200 mm ($ET_U1 \div U3$; Fig. 2b). The instrumental set-up was completed by the measure of the relative displacement between the top chords by means of a suitable potentiometer.

Four further sections were instrumented to measure the vertical displacements at the support and at the span quarters. Finally, one section was instrumented to measure the vertical displacements of the top chords, in order to control the expected instability of the inclined wings at a distance of 2.5 m from the central section. The instrumental equipment consisted of potentiometer transducers connected via a

multiplexer to an Analog/Digital card directly inserted in a PC. The vertical displacement can be affected by a maximum precision error of about 0.1%. By contrast, the longitudinal strains were measured by means of resistive transducers with a lower precision (linearity error less than 0.3%; gauge stroke = 10 mm), but the small values recorded justify the choice made. Each steel bar bundle had a weight in the range of about 9 – 23 kN and was characterized by an eccentricity with respect to the barycentre of the cross section. Due to the long span of these elements, two bundles (each 12 m long) were located on the extrados in the same position on the right and on the left side of the middle section, and for each bundle the eccentricity was measured (with an approximation of about 5 cm). More detailed information can be found in the technical report, where some sliding shear experimental data is also shown (di Prisco & Trintinaglia, 2002).

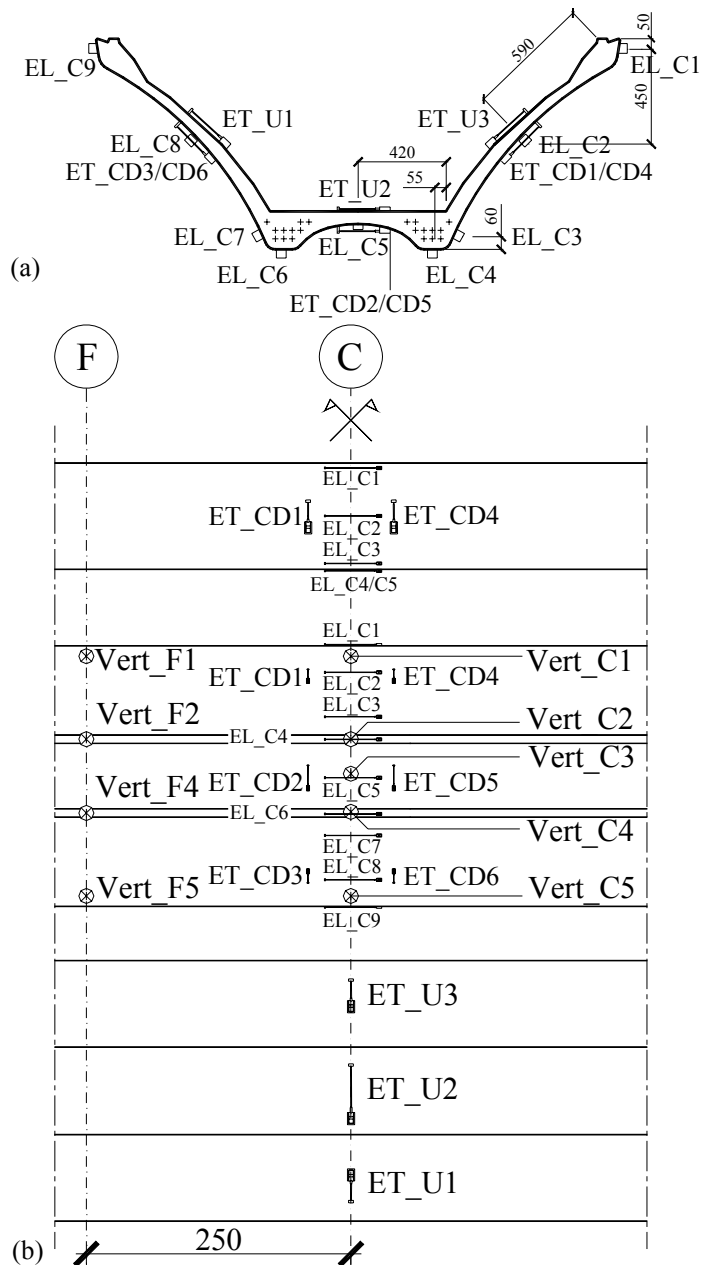


Figure 2. Instrumental equipment in the central segment: (a) cross section view; (b) longitudinal projections.

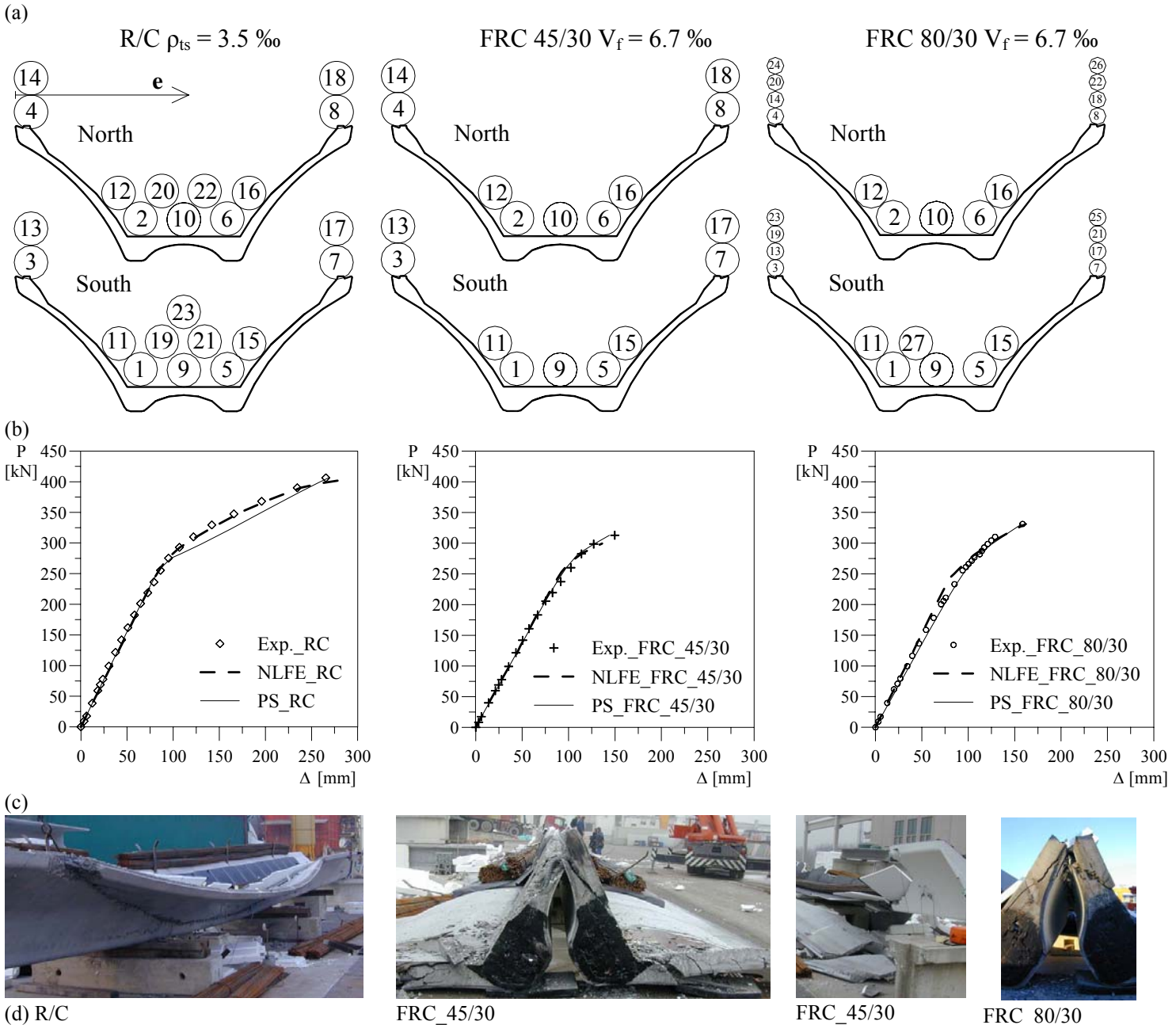


Figure 3. Structural tests: (a) typical loading situation view; (b) steel bundle location, (c) total load vs. midspan deflection measured with bottom LVDTs; (d) collapse views.

In the experimental investigation the steel bundles were maintained on the top chords by six suitable steel forks (Fig.3a). The symmetric load condition is here considered up to collapse, even if at the serviceability conditions the structural element was also loaded with a weak torsion in the test due to bundle eccentricities. In the last step, the vertical displacement (C5) was removed to prevent the transducer failure.

3 MATERIAL CHARACTERISATION

3.1 Mix design

Three materials were analysed. They had similar HPC matrix ($R_{cm} = 73-82$ MPa), characterized by 380 kg/m^3 of cement I 525 and 60 kg/m^3 of fly ash. The w/b ratio was equal 0.34 and the aggregates (120 kg/m^3 of 0-3 mm sand, 970 kg/m^3 of 0-12 mm sand and 815 kg/m^3 8-15 mm gravel) were siliceous. Two fibre reinforced concrete were obtained by add-

ing 50 kg/m^3 of 30 mm long, hooked-end steel fibres: the fibres were made of low or high-carbon steel and were characterized by two different aspect ratio (45 or 80 respectively).

3.2 Mechanical characteristics

The materials were mechanically characterized according to the National Guidelines CNR 11039. In particular, besides the cubic compressive strength, for each fibre reinforced material, also three notched prismatic beams ($150 \times 150 \times 600 \text{ mm}$) were tested according to a 4 point bending test set up, taking the Crack Mouth Opening Displacement (CMOD) as feedback parameter.

Table 1. Experimental mechanical characteristics of materials.

	R_{cm}	$f_{f,m}$	$f_{eq0-0.6m}$	$f_{eq0.6-3m}$	f_{vk}	f_{ptk}
	MPa	MPa	MPa	MPa	MPa	MPa
R/C	82.58	-	-	-	500	1860
45/30	75.65	5.22	5.44	2.80	-	1860
80/30	73.20	5.22	7.56	8.12	-	1860

Table 2. Computed mechanical characteristics of materials.

	E_c	ν	f_c	f_{ct}	σ_a	w_a	σ_b	w_b
	MPa		MPa	MPa	MPa	mm	MPa	mm
R/C	39193	0.2	68.54	5.02	-	-	-	-
45/30	38176	0.2	62.79	4.70	2.45	0.3	0.31	1.8
80/30	37801	0.2	60.76	4.70	3.40	0.3	2.55	1.8

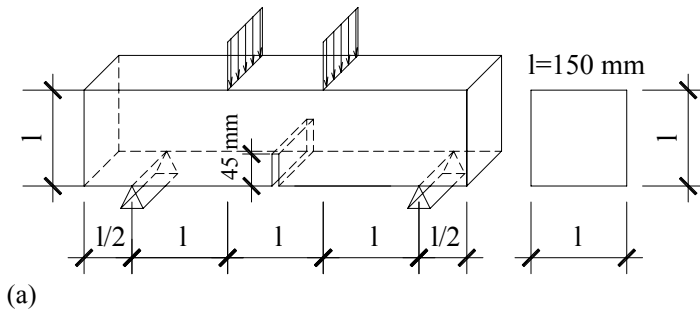


Figure 4. UNI test: (a) geometry and test set-up; (b) specimen image during testing.

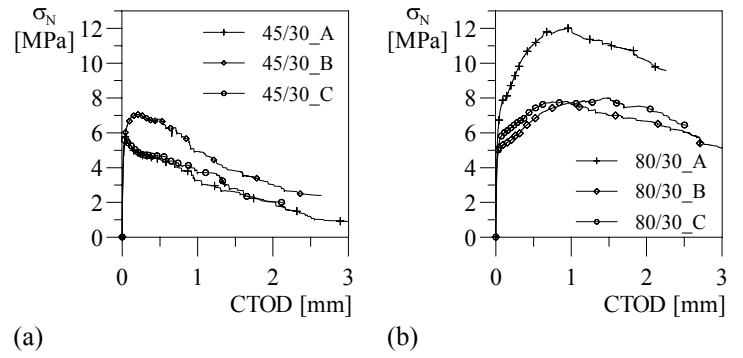


Figure 5. Load vs. CTOD for UNI tests: (a) 45/30; (b) 80/30

The notch/depth ratio of the specimens was 0.3. The first cracking strength (f_{lim}), and the average residual post-cracking strengths in two Crack Tip Opening Displacement ranges were indicated in Table 1: the serviceability ($CTOD = 0-0.6 \text{ mm}$; $\sigma_{0-0.6}$) and the ultimate average values ($CTOD = 0.6 - 3 \text{ mm}$; $\sigma_{0.6-3}$) are both there shown. Finally, the yielding and the ultimate strengths of steel for welded mesh and prestressing reinforcement are indicated. According to Model Code and CNR DT-204, other basic mechanical parameters were computed (Table 2). It is worth to note that the same FRC materials were carefully investigated also by means of an extensive experimental programme aimed at the characterization in uniaxial tension, eccentric tension and simple bending of unnotched prismatic thin specimens, taking into account also size effect in the range 1:6.25 (di Prisco et al., 2004).

4 CONSTITUTIVE LAWS

The modelling adopted, that uses both the plane section model and the shell elements in a Finite Element approach, requires only uniaxial constitutive laws. In fact, in the F.E. approach, the biaxial state of stress is described by means of two equivalent uniaxial states. If 1-2 denote the principal directions of strains, the strength values, corresponding to the “equivalent” uniaxial states, were determined through the analytical biaxial strength envelope suggested by Kupfer (Belletti et al. 2001). Depending on the uniaxial stress-strain curve, the secant moduli E_1 and E_2 are determined and the stiffness matrix for the orthotropic material takes the following form:

$$[D_{i,2}^c] = \frac{I}{1-\nu^2} \begin{bmatrix} E_1 & \nu\sqrt{E_1E_2} & 0 \\ \nu\sqrt{E_1E_2} & E_2 & 0 \\ 0 & 0 & \frac{1}{4}(E_1 + E_2 - 2\nu\sqrt{E_1E_2}) \end{bmatrix} \quad (1)$$

Uncracked reinforced concrete stiffness matrix is obtained by adding to concrete stiffness matrix $[D_{1,2}^c]$ the contribution of i -th steel bars, assumed smeared and inclined by an angle $\varphi_i = \theta_i - \psi$, where θ , ψ indicate the steel axis and the 1 principal direc-

tion in relation to x axis, respectively, with respect to 1 axis:

$$[D_{1,2}] = [D_{1,2}^c] + [D_{1,2}^s] = [D_{1,2}^c] + \sum_{i=1}^n [T_{(\varphi_i)}^t] [D_{si}] [T_{(\varphi_i)}] \quad (2)$$

being:

$$[T_{(\varphi_i)}] = \begin{bmatrix} c_i^2 & s_i^2 & c_i s_i \\ s_i^2 & c_i^2 & -c_i s_i \\ -2c_i s_i & 2c_i s_i & c_i^2 - s_i^2 \end{bmatrix} \quad [D_{si}] = \begin{bmatrix} \rho_i E_{si} & 0 & 0 \\ 0 & 0 & 0 \\ 0 & 0 & 0 \end{bmatrix}$$

$$c_i = \cos \varphi_i \quad s_i = \sin \varphi_i$$

When the principal tensile stress, calculated at the integration point, becomes greater than the concrete tensile strength, crack occurs and the procedure adopts the stiffness matrix for cracked reinforced concrete, having orthotropic axes coincident with the direction perpendicular, 1, and parallel, 2, to the fixed crack. The strain field is expressed as a function of three fundamental variables: the crack width w , the crack slip v and the concrete axial strain ε_{c2} in the direction parallel to the crack. The strain vector, expressed in the orthotropic co-ordinate system, takes the following form:

$$\{\varepsilon_{1,2}\} = \{\varepsilon_1 \quad \varepsilon_2 \quad \gamma_{12}\}^t = \left\{ \frac{w}{a_m} \quad \varepsilon_{c2} \quad \frac{v}{a_m} \right\}^t$$

a_m being the crack spacing, assumed constant and depending on rebar spacing.

The stiffness matrix of cracked reinforced concrete takes into account all the fundamental phenomena occurring after cracking, such as tension stiffening, dowel action, bridging effect, confinement and aggregate interlock (Belletti et al. 2001). The constitutive relationship adopted for steel is represented by the bilateral elastic-hardening curve, while for concrete in compression the softened Thorenfeld curve has been implemented. The stiffness matrix, both for uncracked and cracked concrete, is referred to the 1-2 orthotropic coordinate system, and a fixed crack approach is followed.

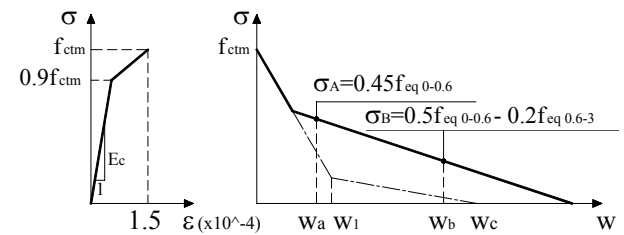
Under loading, if the minor principal moment reaches cracking moment values (i.e. as happens in the wings and in the bottom slab for the analysed precast element), two sets of primary and secondary cracks may occur at the integration point. Following the same approach proposed in (Belletti et al. 2003), in R/C case doubly cracked concrete is assumed to have zero secant Young's modulus in the direction parallel to the first crack, after the peak, while reduced softening is taken into account for FRC cases.

4.1 Constitutive relationships for the material

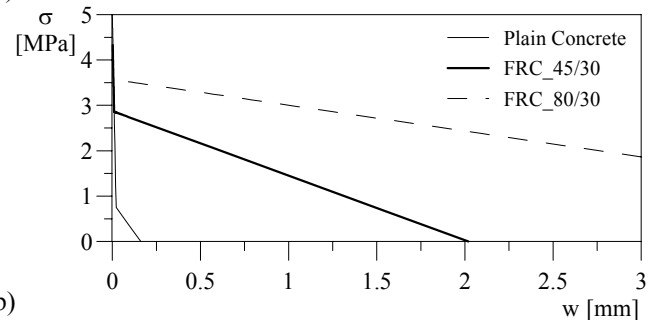
The uniaxial constitutive laws assumed for plain concrete material were those suggested in Model Code: Sargin equation for uniaxial compression and

the trilinear relation for uniaxial tension (Fig.6a). According to Model Code, the values w_1 and w_c are function of fracture energy that is related to the maximum aggregate size and the cylindrical compressive strength: the computed values are respectively 21 and 161 μm .

FRC materials adopt the same constitutive law in uniaxial compression due to the small fibre content, while in uniaxial tension only the final branch is substituted according to CNR DT-204 (di Prisco et al., 2004a,b; Fig.6a) in order to suitably take into account pull-out mechanism. The significant increase of dissipated energy due to fiber addition is immediately perceived by observing the softening laws (Fig.6b). According to the experimental data, there is a significant difference between the two types of steel fibre.



(a)



(b)

Figure 6. Uniaxial tension constitutive relationships: (a) general description; (b) σ - w curves adopted for the materials.

4.2 Generalized constitutive relationships

According to plane section model, that is the smeared version of the multi-layer procedure first introduced by Hordjik (1991; see also di Prisco et al. 2001), the bending moment vs. curvature curve for the softened region in R/C and FRC thin walled plates was computed. The structural characteristic length l_c , representing the size of the softening region, was assumed equal to the crack distance and the plate thickness for R/C and FRC elements respectively.

The results (Fig.7) highlight as R/C element is characterized by a reinforcement ratio larger than the minimum in the central section, but not at the connection between the wing and the bottom chord. On the contrary, SFRC bending behaviour appears almost elasto-plastic, even though sometimes this is not enough to guarantee a multi crack pattern. The comparison with the results of a previous bending

characterization of the same material on unnotched plates (di Prisco et al, 2004a) gives a reliable fitting.

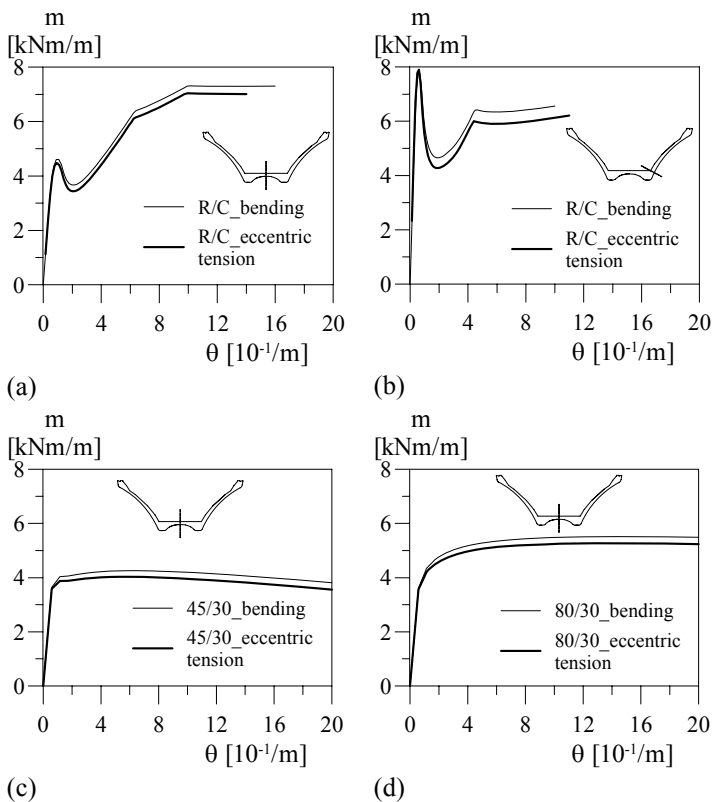


Figure 7. Bending moment vs. average curvature: current longitudinal cross section (width =1m): (a) R/C along the symmetric plane; (b) R/C at the inclined wing – bottom slab connection; (c) SFRC 45/30 along the symmetric plane; (d) SFRC 80/30 along the symmetric plane.

5 STRUCTURAL MODELLING

The anticipated failure of the structural tests presented were predicted by investigating the crosswise bending with a second-order approach. According to this approach (di Prisco et al., 1998, 2002), that regards each longitudinal fibre as a wire, an additive distributed load can be computed by multiplying the longitudinal curvature times the longitudinal stress acting on the cross section (Fig. 8a) Each statical contribution is evaluated on the basis of the equilibrium of a beam longitudinal segment, by assuming that the projection of the cross-section cannot deform itself in its plane. Therefore, besides the external load contribution offered by self-weight and steel bundles (Fig. 8b), second-order effects associated to the main longitudinal curvature are also taken into account.

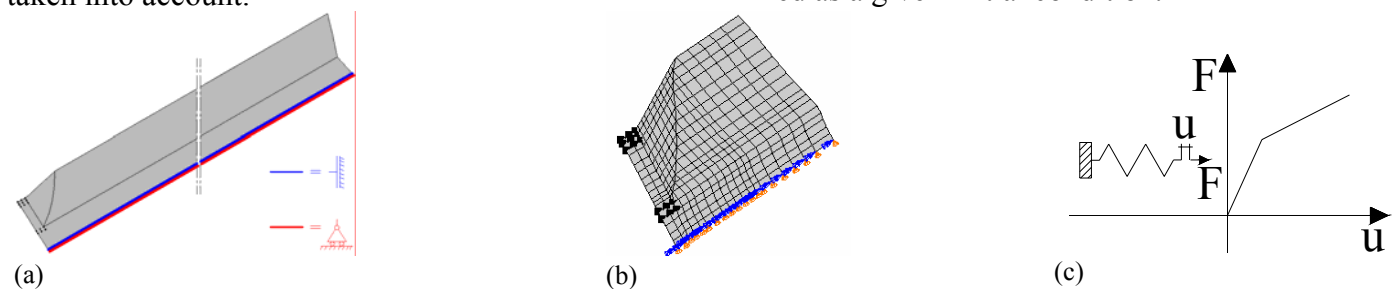


Figure 9. (a) Mesh adopted for NLFEA; (b) a zoom of the closed end; (c) no-tension spring element adopted as support condition.

The superposition is strictly valid up to first cracking. The longitudinal stresses caused by longitudinal bending can be evaluated also for cracked section according to a plane-section model and a perfect compatibility between concrete and steel ($\epsilon_s = \epsilon_c$); in this way the main mechanical non-linearity can be taken into account. The shear flows $q_i(s)$ are distributed according to Jourawski's theory; the specific torque $m_{DSV}(s)$, is computed according to circular torsion owing to the large values of the warping factor (Vlasov, 1961), estimated only by taking into account the uncracked portions of the cross-section. The equilibrium allows us also to compute the shear (v_s) and the axial force (n_{ss}) along the wing profile (Fig.8b).

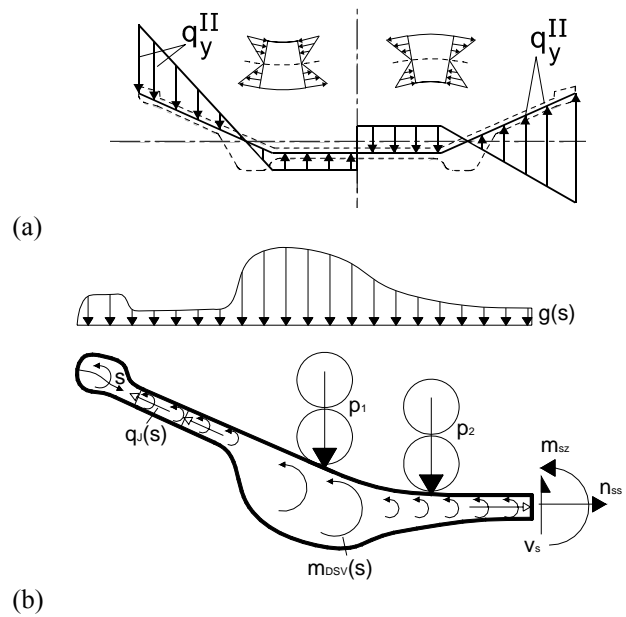


Figure 8. Second-order plane-section model [di Prisco et al.2002]: (a) transverse bending introduced by second-order distributed loads for thin-walled open sections and (b) equilibrium according to Vlasov approach.

The total crosswise bending moment (m_{sz}) can be compared with the resistant one. With reference to F.E. approach, due to the symmetry in the geometry, as well as in the loading along the cross-section and support conditions, only half of the cross section was modelled for the entire length of the element (Fig. 9a). The support condition (Fig. 9b) was modelled through spring elements having no tension behaviour (Fig. 9c). Rebar layers, embedded in the “host” shell elements, were used in order to model strands. The prestressing action in the rebars was defined as a given initial condition.

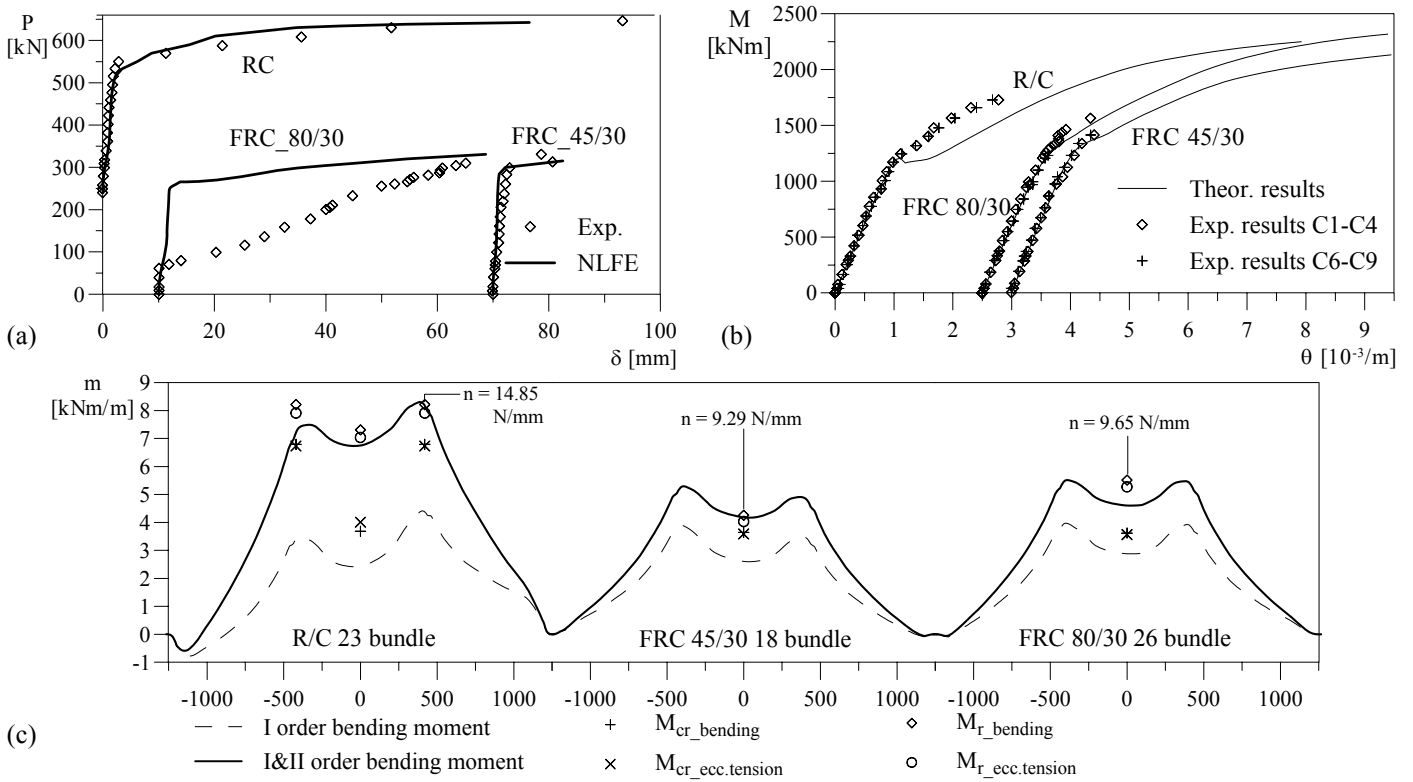


Figure 10. Longitudinal and transverse behaviour of the three prefabricated structures: (a) load vs. transverse opening of the wings; (b) bending moment vs. longitudinal curvature; (c) transverse bending moment along the curvilinear abscissa.

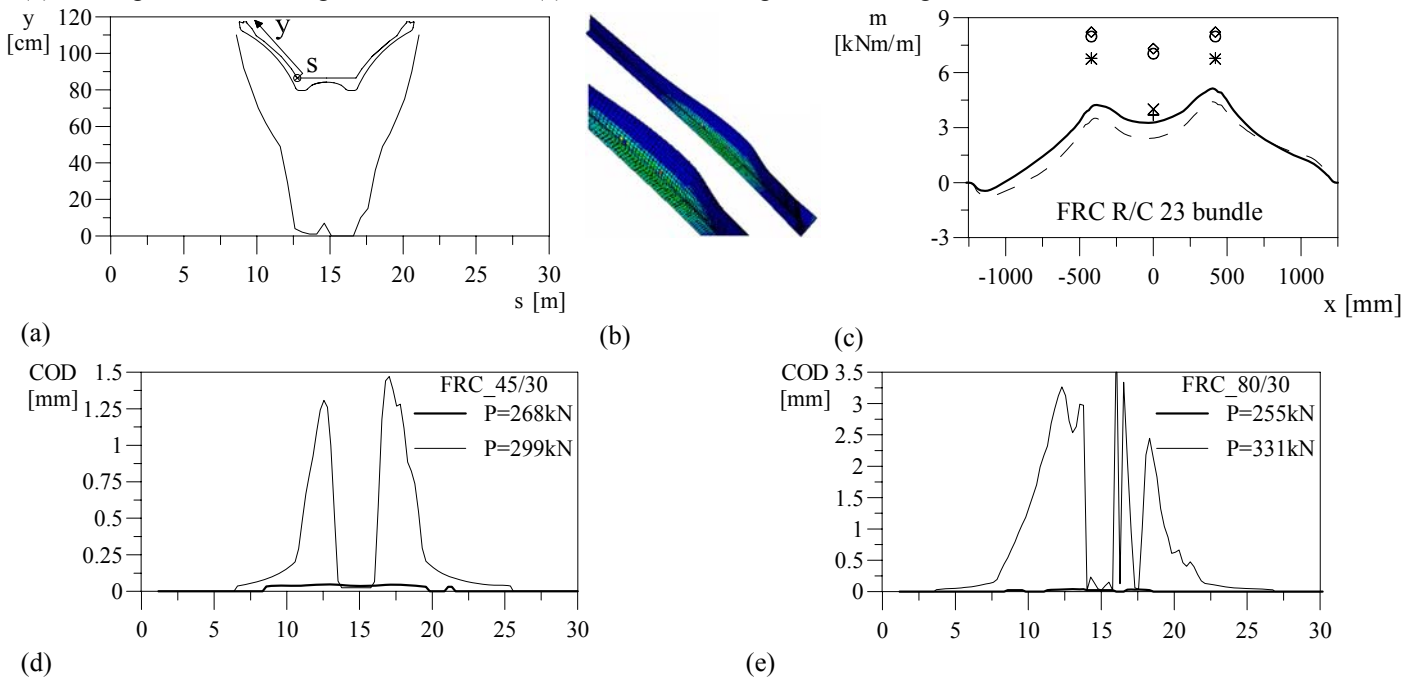


Figure 11. (a) fracture profile in the wing measured along the longitudinal axis; (b) F.E. deformed shape at failure; (c) transverse bending moment in a section at 9 m from the support; F.E. approach: crack opening along the longitudinal axis for (d) 45/30 and (e) 80/30 SFRC elements.

In F.E. modelling, the related distributed load was concentrated in six loads acting on each top chord, while in the simple model these bundles were regarded as longitudinally distributed load strips according to the eccentricities experimentally measured, and therefore, along the cross-section profile each bundle was regarded as a specific concentrated load.

The F.E. prediction expressed in terms of load vs. crosswise opening of the wings measured in the midspan fits very well the experimental curves

(Fig.10a); only the experimental behaviour of 80/30 FRC element seems to be affected by a previous crack pattern that can be expected in such a long element. This defect transforms a predicted abrupt opening of the inclined wing in a progressive phenomenon, without changing the asymptotic load value. Furthermore, the good fitting of the crosswise cracking in the other two cases was obtained by a reduction of 15% of the average peak strength, that can be associated to the statistical strength reduction due to small defects distributed in the central zone. The plane section model clarifies the significant

section model clarifies the significant reduction in terms of longitudinal bending moment, due to the crosswise failure of the section (Fig. 10b), although the lack of tension stiffening effects in the model causes larger curvatures after cracking in the prediction. The crosswise equilibrium analysis of the section at the last experimental load step (Fig. 10c) highlights the reliability of this design approach as well as the key role of second order effects in the crosswise bending.

The deformed shape of R/C element is very well reproduced by F.E. modelling (Figs. 11a,b), but also an equilibrium analysis of a cross section performed by means of the plane section model at the border of the fracture profile, at 9 m from the supports, shows the strong reduction of the bending moment crosswisely acting on the wing/bottom chord connection, moving from the midspan towards the supports. Second order effects are also highlighted by the crack opening of the extrados bottom plate measured along the longitudinal axis (Figs. 11d,e). Also in this case, the crack propagation from the centre towards the supports emphasizes second order effects, taking into account also the lack of steel bundles in the midspan for about a 1m long segment.

6 CONCLUSIONS

Finite Element modelling of R/C and FRC structural elements is able to predict the deformation and the failure mechanisms, experimentally observed, up to the last load-step; the only exception concerns 80/30 FRC element, where an existing longitudinal crack anticipated the wing opening without significant changes on the ultimate load, due to tensile residual strength guaranteed by fibre pull-out. Second order effects significantly affect these structural elements: the very brittle failure observed was also emphasized by the lack of one closed end, that prevents an alternative equilibrium condition due to torsional resistance. The good fitting of the structural behaviour for R/C and 45/30 FRC elements confirms the reliability of the constitutive relationships chosen for the materials and suggests quite negligible influence of size effect on both the matrix and the residual strengths. The plane section model gives a reliable instrument to capture second order effects, even it could be weakly unsafe, because it does not take into account the limited deformability in the cross section plane. The strong reduction of the longitudinal bending moment capacity computed with reference to the average strength values (from 23% for R/C element up to 38% for 45/30 FRC element!), highlights the need for such element of higher crosswise bending resistance in the central regions, attainable with larger reinforcement ratios, increased fibre contents or special ties and suitable closed ends.

REFERENCES

- Belletti, B., Cerioni, R. & Iori, I. 2001. A Physical Approach for Reinforced Concrete (PARC) membrane elements. *J. Struct. Engrg., ASCE*, 127 (12), 1412-1426.
- Belletti, B., Cerioni, R. & Iori, I. 2002. Theoretical and Experimental Analyses of Precast Prestressed Concrete Roof Elements for Large Span. *First fib Congress, Osaka*, on CD ROM.
- Belletti, B. 2002. Nonlinear FE analysis of precast prestressed concrete roof elements (in italian). *Proc. of 14° Congress CTE, Mantova*, 13-22.
- Belletti, B., Bernardi, P., Cerioni, R. & Iori, I. 2003. Non-linear analysis of reinforced concrete slabs. *Proceedings of ISEC-02 Conference*, 663-668.
- Belletti, B., di Prisco, M. & Dozio, D. 2006. Thin-webbed Open Cross-section Roof Elements: Modelling of Second Order Effects up to Failure, *Proc. of the 2nd fib Congress, Napoli (Italy), June 5-8*, ID 3-69 on CD-ROM.
- CNR-DT 204, 2006. Guidelines for the design, construction and production control of the fibre reinforced concrete structures.
- di Prisco, M., Felicetti, R. & Ferrara, L. 1998. Mono-cellular element for large-span roof: a theoretical and experimental investigation (in Italian), *Proc. of 12° CTE Conference, Padova*, 525-535.
- di Prisco, M. & Felicetti, R. 1999. HSC Thin-Web Roof-Elements: an Experimental Investigation on Steel fibre Benefits. *Proc. 5th Int. Symposium on Utilization of HS/HP Concrete, Sandefjord, Norway*: 546-555.
- di Prisco, M., Felicetti, R., Iorio, F. & Gettu, R. 2001. On the identification of SFRC tensile constitutive behavior. In R. de Borst, J.Mazars, G. Pijaudier-Cabot & J.G.M. van Mier (eds.), *Fracture Mechanics of Concrete Structures*: 541-548. A.A. Balkema Publishers.
- di Prisco M. & Trintinaglia, C. 2002. Investigation on the structural behaviour of precast prestressed roof elements – TP elements. *Technical report DIS Politecnico di Milano*.
- di Prisco, M., Iorio, F., Trintinaglia & C., Signorini, S. 2002. Thin-web open-section roof elements: geometrical non linearity effects, (in Italian), *Proceedings 14° CTE Conference, Mantova*: 569-578.
- di Prisco, M., Iorio, F. & Plizzari, G. 2003. HPSFRC prestressed roof elements. In B. Schnütgen and L. Vandewalle (eds.), *Test and Design Methods for Steel Fibre Reinforced Concrete – Background and Experiences*, PRO31: 161-188. Bochum: Rilem Publications S.A.R.L..
- di Prisco, M., Felicetti, R., Lamperti M. & Menotti, G. 2004a. On size effect in tension of SFRC thin plates. *Fracture Mechanics of Concrete Structures*, (eds.). In V.C. Li C.K.Y.Leung, K.J.Willam, S.L. Billington (eds.) vol.2: 1075-1082. B.L.Schmick & A.D.Pollington Publishers.
- di Prisco, M., Ferrara, L., Colombo & M., Mauri, M. 2004b. On the identification of SFRC constitutive law in uniaxial tension, in Fibre-reinforced concretes. In M. di Prisco, R. Felicetti, G.A. Plizzari (eds.), *Fiber reinforced concrete - BEFIB*: 827-836. Cahan: Rilem Publications S.A.R.L.
- di Prisco, M. & Dozio, D. 2005. Thin-webbed open cross-section roof elements: second order effects. *Proceedings of the International FIB Symposium Keep concrete attractive, Budapest, May 23-25*: 619-624.
- Hordijk, D. 1991. Local approach to fatigue of concrete, Ph.D.Thesis, Delft University of Technology, 1-207.
- UNI 11039 2003. Steel fibre reinforced concrete. Test method for the determination of first crack strength and ductility indexes.
- Vlasov, V.Z. 1961. Thin walled elastic beams, Israel Programme for Scientific Translation, Jerusalem (1961).